Mon. Not. R. Astron. Soc. **351,** 1121–1133 (2004) doi:10.1111/j.1365-2966.2004.07865.x

Accretion dynamics in neutron star–black hole binaries

S. Rosswog,[1,2]★ R. Speith[3,2] and G. A. Wynn[2]

[1]*School of Engineering and Science, International University Bremen, Germany*
[2]*Department of Physics and Astronomy, University of Leicester*
[3]*Institut für Astronomie und Astrophysik, Universität Tübingen, Germany*

Accepted 2004 March 22. Received 2004 March 19; in original form 2004 March 3

ABSTRACT

We perform three-dimensional, Newtonian hydrodynamic simulations with a nuclear equation of state to investigate the accretion dynamics in neutron star–black hole systems. We find as a general result that non-spinning donor stars yield larger circularization radii than corotating donors. Therefore, the matter from a neutron star without spin will more likely settle into an accretion disc outside the Schwarzschild radius. With the stiff equation of state used we find it hard to form an accretion disc that is promising to launch a gamma-ray burst. In all relevant cases the core of the neutron star survives and keeps orbiting the black hole as a mini neutron star for the rest of the simulation time (up to several hundred dynamical neutron star time-scales). The existence of this mini neutron star leaves a clear imprint on the gravitational wave signal which thus can be used to probe the physics at supranuclear densities.

Key words: accretion, accretion discs – dense matter – methods: numerical – stars: neutron.

1 INTRODUCTION

Neutron star–black hole binaries are thought to be excellent candidates for ground-based gravitational wave (GW) detection (e.g. Belczynski, Kalogera & Bulik 2002, and references therein). If their true coalescence rate is close to the upper end of the estimated values, neutron star–black hole systems may be among the first sources detected. They are further – together with double neutron star systems – the favoured model for the subclass of short gamma-ray bursts (GRBs; Paczynski 1992; Narayan, Pazcynski & Piran 1992); a coincident detection of a GW 'chirp' signal together with a GRB could be the ultimate proof for the compact binary nature of the short GRB progenitors. Moreover, the cold decompression of nuclear matter by the tidal disruption of a neutron star has been considered as a possible production site of rapid neutron capture elements (Lattimer & Schramm 1974, 1976; Lattimer et al. 1977; Symbalisty & Schramm 1982; Eichler et al. 1989; Rosswog et al. 1999; Freiburghaus, Rosswog & Thielemann 1999).

Full general relativistic simulations of this event are very challenging as apart from the complicated neutron star physics the dynamic evolution of the space–time must also be followed since the systems of interest have comparable masses for both binary components and therefore a fixed space–time cannot be assumed. But the dynamics of the event is demanding enough even if treated in the Newtonian approximation. Simulations of neutron star–black hole encounters have been described in a series of papers by Lee and Lee and Kluzniak (Lee & Kluzniak 1999a,b; Lee 2000, 2001). They used three-dimensional (3D) smoothed particle hydrodynamics, Newtonian self-gravity plus back-reaction forces from GW emission and polytropic equations of state (EOS) of varying stiffness. Janka et al. (1999) performed neutron star–black hole merger calculations using a 3D Piecewise Parabolic Method (PPM) code, again using Newtonian self-gravity plus back-reaction forces, but with the nuclear EOS of Lattimer & Swesty (1991) and a detailed neutrino treatment (Ruffert, Janka & Schäfer 1996).

The focus of our investigation in this paper is the complex accretion dynamics in a neutron star–black hole system. Many of the (analytical) approximations that are successfully used in other accreting systems are of only limited value in this context. For example, the Roche potential of point mass binaries is only a rough approximation to the neutron star with its rather flat density profile; neutron star–black hole binaries are most likely not corotating like other close binaries (Bildsten & Cutler 1992) and, owing to their tiny pressure scale heights in the neutron star surface, 'standard' estimates of the distance where mass transfer sets in can only give a very rough guideline.

We present in Section 2 analytic estimates that explain why irrotational donor stars do generally form accretion discs easier than corotating donors. We explain in Section 3 our numerical methods and initial conditions, results concerning the accretion dynamics and the corresponding GW emission are presented in Section 4. In Section 5 we summarize our results.

2 ANALYTIC ESTIMATES

While the GW signature is predominantly determined by the bulk motion of the event, the neutrino and electromagnetic signals from a neutron star–black hole system require an accretion disc to form.

★E-mail: s.rosswog@iu-bremen.de

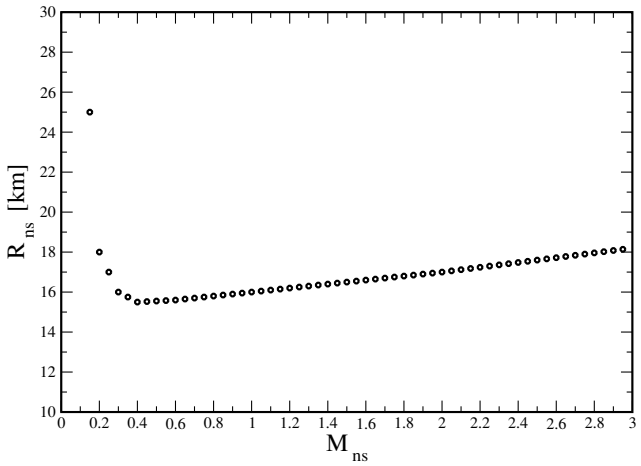

Figure 1. Mass–radius relationship for the Shen EOS used: for neutron star masses above 0.4 $M_\odot$ the neutron star will shrink upon mass loss, below this value it will increase its radius.

Moreover an accretion disc is thought to be an indispensable ingredient for a GRB central engine (e.g. Piran 1999; Mészáros 2002). Therefore we explore with simple analytical formulae the conditions under which a disc can form.

We want to point out the fact that the following estimates only are illustrative in character as they are very approximate for two reasons: first, the used formulae refer to Roche geometry, i.e. to the gravity of point masses, while the stiff neutron star EOS leads to an almost uniform mass distribution inside the neutron star. Secondly, and more importantly, the stiff neutron star EOS results in tiny pressure scale heights in the neutron star surface and therefore the level of uncertainty in the estimate of the Roche radius can easily correspond to several orders of magnitude in terms of pressure scale heights.

The dynamics of how the mass transfer proceeds depends crucially on the way the neutron star reacts on mass loss, i.e. whether it shrinks or expands. The mass–radius relationship of a polytropic neutron star with adiabatic exponent Γ is given by (e.g. Kippenhahn & Weigert 1990)

$$R \propto M^{(\Gamma-2)/(3\Gamma-4)}, \tag{1}$$

i.e. for $\Gamma = 2$ the radius is independent of the mass and for larger (smaller) values the neutron star shrinks (expands) on mass loss. For a realistic nuclear EOS Γ is density dependent (for an example see the comparison between the Shen- and the Lattimer–Swesty EOS in Rosswog & Davies 2002, fig. 5) and therefore the reaction of the neutron star on mass loss depends on its current mass. The mass–radius relationship of the used Shen EOS is given in Fig. 1. Above 0.4 $M_\odot$ a neutron star will shrink upon mass loss, below this value its radius increases.

2.1 Accretion disc formation: dependence on donor spin

We show that – and explain why – it is in general easier to form an accretion disc owing to Roche lobe overflow, if the donor star is non-rotating rather than being tidally locked. In the non-rotating case, matter flowing across the Lagrange point L_1 has a larger specific angular momentum and therefore yields a larger circularization radius than in the corotating case. As a consequence, in the first case more matter can form an accretion disc outside the Schwarzschild radius, while for a corotating donor the bulk of material is fed directly into the hole.

For the sake of simplicity we assume in the following that the Roche potential is a valid approximation for our purposes. We further neglect radial velocities of the binary components and tidal deformations and lag angles of the donor star. Generally, the circularization radius is an estimate for the initial disc size. It is proportional to the square of the specific angular momentum, l_{L_1}, of the accretion stream at the L_1 point as measured in a coordinate system (Σ) with non-rotating axes and the origin centred on the black hole

$$R_{\rm circ} = l_{L_1}^2/(GM_{\rm BH}), \tag{2}$$

where $M_{\rm BH}$ is the mass of the black hole. Therefore, we have to show that the irrotational case yields a larger value for l_{L_1}, i.e. $l_{L_1}^{\rm irr} > l_{L_1}^{\rm corr}$. The specific angular momentum is defined as $\boldsymbol{l}_{L_1} = \boldsymbol{b}_1 \times \boldsymbol{v}_{L_1}$, where $\boldsymbol{b}_1$ is the vector from the black hole to the L_1 point. The velocities at the L_1 point are easiest found in a coordinate system (Σ') corotating with the binary centred around the black hole. Here and in the following, all unprimed quantities refer to Σ, while primed ones refer to Σ'. The coordinate transformation between the two systems is given by

$$\boldsymbol{x} = R_\varphi \boldsymbol{x}' \tag{3}$$

$$\boldsymbol{v} = \boldsymbol{\omega} \times \boldsymbol{x} + R_\varphi \boldsymbol{v}', \tag{4}$$

where R_φ is the matrix describing a rotation around $\boldsymbol{\omega}$. The rotation angle φ is given by ωt, where $\omega = |\boldsymbol{\omega}|$ is the binary orbital angular velocity.

For a corotating donor star all the fluid velocities vanish in the corotating frame Σ', i.e. $\boldsymbol{v}' = 0$. Hence, the velocity at L_1 in Σ reads

$$\boldsymbol{v}_{L_1} = \boldsymbol{\omega} \times \boldsymbol{b}_1 \tag{5}$$

and therefore

$$\boldsymbol{l}_{L_1}^{\rm corr} = b_1^2 \boldsymbol{\omega}. \tag{6}$$

An irrotational donor star, however, appears in Σ' to be spinning against the orbital motion with $\omega_{\rm spin} = -\omega$,

$$\boldsymbol{v}'_{L_1} = -\boldsymbol{\omega} \times (\boldsymbol{b_1}' - \boldsymbol{a}'), \tag{7}$$

where $\boldsymbol{a}'$ denotes the vector pointing from the black hole to the neutron star. Inserting equation (7) into equation (4) and considering equation (3) leads to

$$\boldsymbol{v}_{L_1} = \boldsymbol{\omega} \times \boldsymbol{a} \tag{8}$$

and finally

$$\boldsymbol{l}_{L_1}^{\rm irr} = b_1 a \boldsymbol{\omega}. \tag{9}$$

Obviously, as $l_{L_1}^{\rm irr} > l_{L_1}^{\rm corr}$, we have

$$R_{\rm circ}^{\rm irr} > R_{\rm circ}^{\rm corr}. \tag{10}$$

Using equation (2) and Kepler's third law the circularization radii can be written as

$$R_{\rm circ}^{\rm corr} = (1+q) b_1 \Big/ \left(\frac{b_1}{a}\right)^3 \tag{11}$$

$$R_{\rm circ}^{\rm irr} = (1+q) b_1 \Big/ \left(\frac{b_1}{a}\right), \tag{12}$$

where $q = M_{\rm NS}/M_{\rm BH}$ ($M_{\rm NS}$ is the neutron star mass). We now assume that mass transfer sets in once the (unperturbed) neutron star radius, $R_{\rm NS}$, is comparable to its Roche radius. The accretion stream from the neutron star to the black hole will result in a disc if the stream tries to settle outside the Schwarzschild radius of the hole, $R_{\rm SS}$, i.e. if $R_{\rm circ} > R_{\rm SS}$. We plot in Fig. 2 the conditions under which a disc can form, for both the corotating and the irrotational

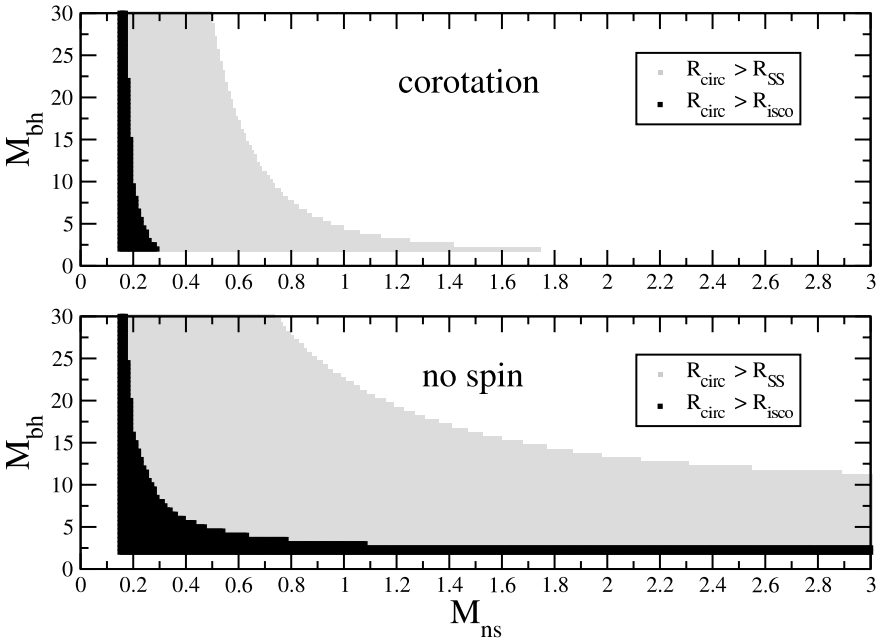

Figure 2. The conditions under which an accretion flow from the neutron star will settle into an accretion disc, i.e. $R_{\rm circ} > R_{\rm SS}$ (grey-shaded). We also show (in black) the masses for which the circularization radius is outside the last stable orbit, $R_{\rm isco} = 6\,M_{\rm BH}$. The upper panel refers to the case of a corotating donor star, while the lower is for a neutron star without spin.

cases. To produce the plot we have used the formula of Plavec & Kratochvil (1964) to estimate b_1, the Roche radius is approximated according to Eggleton (1983), and for the radius of the neutron star as a function of mass we use the (cold, $T = 0$) EOS of Shen et al. (1998a,b); see Fig. 1. The grey-shaded area refers to the condition $R_{\rm circ} > R_{\rm SS}$ and the black area to $R_{\rm circ} > R_{\rm isco} = 6\,M_{\rm BH}$. $R_{\rm isco}$ is the radius of the innermost, stable circular orbit of a test particle around a Schwarzschild black hole.

Although these are just rough estimates, Fig. 2 clearly shows how difficult it is to form an accretion disc for a corotating 1.4 $M_\odot$ neutron star: only for extremely low-mass black hole cases (2 $M_\odot$) will the accretion stream settle in a disc around the hole. In the more realistic case of a more massive hole the accretion stream will be fed directly into the hole and only form a disc once the neutron star has expanded on mass loss. In the irrotational case, however, the fraction of the parameter space that allows for an accretion disc formation is much larger. From a 1.4 $M_\odot$ neutron star an accretion disc will form even for a black hole as massive as $\sim$18 $M_\odot$.

All these results are generally confirmed by the set of numerical simulations presented in Section 4.

3 MODEL

3.1 Numerical method

We solve the equations of fluid dynamics in 3D using a Lagrangian particle scheme (smoothed particle hydrodynamics, SPHs; see e.g. Benz 1990; Monaghan 1992). For details of the equations (symmetrization etc.) we refer to the review by Benz (1990). Rather than the 'standard' artificial viscosity (Monaghan & Gingold 1983) we use (Rosswog et al. 2000) time-dependent viscosity parameters that essentially vanish in the absence of shocks, together with the so-called 'Balsara switch' (Balsara 1995) to suppress spurious viscous forces in pure shear flows. For further details of the implementation we refer to Rosswog & Davies (2002). The Schwarzschild radius is treated as an absorbing boundary, i.e. particles that cross the boundary are removed from the simulation. Their mass and linear momentum are added to the hole in a way that the total centre of mass is conserved. The microphysics of the neutron star fluid is described using a temperature and composition dependent nuclear EOS, based on relativistic mean field theory (Shen et al. 1998a,b; Rosswog & Davies 2002). Local neutrino cooling and compositional changes of the neutron star matter owing to weak interactions are accounted for by a detailed, multiflavour neutrino scheme (Rosswog & Liebendörfer 2003). Details concerning the neutrino emission will be presented elsewhere.

We use Newtonian self-gravity for the fluid which we evaluate via a binary tree. The black hole is treated as a Newtonian point mass, results for pseudo-potentials mimicking relativistic effects will be presented in a forthcoming paper. For the back reaction on to the fluid flow resulting from the emission of GWs we use the formalism of Zhuge, Centrella & McMillan (1996), applying the forces only to SPH particles that have a mass density in excess of a threshold (10^{14} g cm^{-3}), which is above the phase transition density to neutron star matter. This procedure is well justified, as in all but one of our simulations a neutron star core survives which is, to a good approximation, spherically symmetric. In the case of a complete disruption no back-reaction force is applied by construction. This is also well justified, as the matter distribution for this case is very close to axisymmetry.

3.2 Initial conditions

It is a vital ingredient for these calculations to start out from initial conditions that are as accurate as possible as the whole dynamical evolution is sensitive to the starting configuration.

As the neutron star viscosity is too low to lead to a tidal locking of the system during the short interaction time, this spin configuration is not a realistic one (Bildsten & Cutler 1992). It is, however, straightforward to construct such *corotating equilibrium initial configurations*, a fact that makes these conditions appealing. We use the full 3D code to construct the initial particle distributions. This is

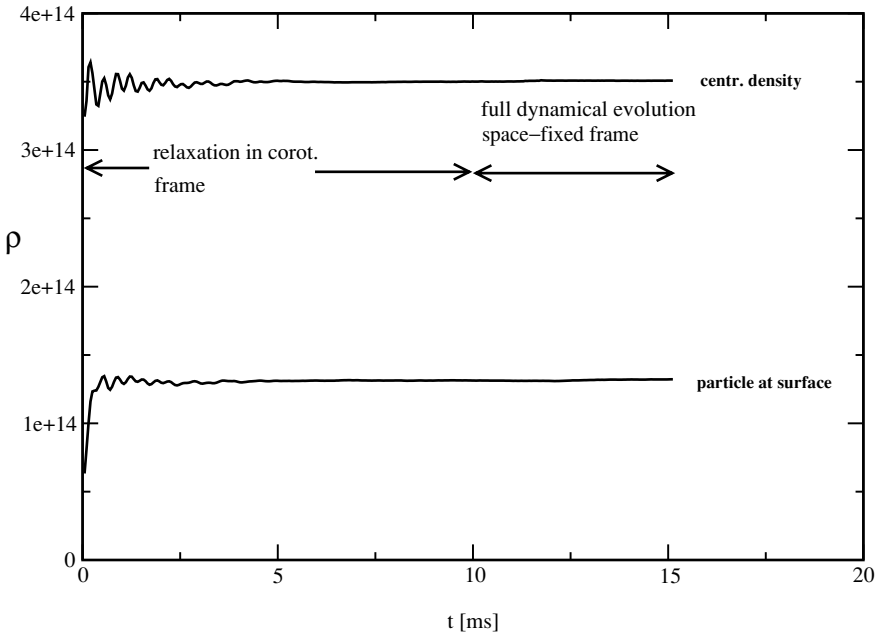

Figure 3. Demonstration of the accuracy of our corotating initial conditions. Shown is the evolution of the central density (in cgs units) and the density of an SPH-particle at the neutron star surface. During the first 10 ms the system is damped (in the corotating frame) into equilibrium, it is then transformed to the space-fixed frame. Subsequently a full simulation of one orbit is performed. The system remains perfectly in the desired equilibrium.

done in the corotating frame as here all the fluid velocities vanish. The relaxation is performed in the following steps.

(i) Calculate the gravitational and hydrodynamic forces, $\boldsymbol{f}_{g,i}$ and $\boldsymbol{f}_{h,i}$, on each particle i using the full hydrocode.

(ii) Determine the resulting force on the centre of mass of the neutron star

$$\boldsymbol{f}_{\mathrm{cm,NS}} = \frac{\sum_i m_i(\boldsymbol{f}_{g,i} + \boldsymbol{f}_{h,i})}{M_{\mathrm{NS}}}. \tag{13}$$

As our neutron star is located on the positive x-axis (origin at the centre of mass), this force will point in the negative x direction.

(iii) To obtain a circular orbit, this force on the centre of mass has to be balanced exactly by the centrifugal forces on the centre of mass, which yields a condition for the rotation frequency, i.e.

$$\omega = \sqrt{\frac{|\boldsymbol{f}_{\mathrm{cm,NS}}|}{M_{\mathrm{NS}} a_{\mathrm{NS}}}}, \tag{14}$$

where a_{NS} is the distance of the neutron star from the origin.

(iv) Now the non-inertial forces are added

$$\boldsymbol{f}_i = \boldsymbol{f}_{g,i} + \boldsymbol{f}_{h,i} - \boldsymbol{\omega} \times (\boldsymbol{\omega} \times \boldsymbol{r}_i), \tag{15}$$

where $\boldsymbol{r}_i$ is the position vector of particle i. Note that we have omitted the Coriolis force as it does not contribute to finding the final corotating state. The addition of the Coriolis force during the relaxation process would only introduce an additional lateral oscillation and therefore increase the computing time to find the equilibrium state.

(v) Finally, we apply an additional velocity proportional friction term to force the system into the corotating state, i.e.

$$\boldsymbol{f}_i = \boldsymbol{f}_{g,i} + \boldsymbol{f}_{h,i} - \boldsymbol{\omega} \times (\boldsymbol{\omega} \times \boldsymbol{r}_i) - \frac{\boldsymbol{v}_i}{\tau}, \tag{16}$$

where τ is a damping time-scale.

(vi) Once equilibrium is achieved, the velocities are transformed back to the space fixed system and the radial velocities are added.

An example of such a relaxation process for a 1.4-$\mathrm{M}_\odot$ neutron star and a 2.8-$\mathrm{M}_\odot$ black hole is shown in Fig. 3. In the first 10 ms the system is relaxed in the corotating frame. Then it is set to an orbit without radial velocities and no back-reaction forces are applied. Subsequently it is evolved for more than one orbital revolution with the full hydro code. The system remains in perfect equilibrium: no oscillation in the densities of the centre and the surface can be seen, after one orbit practically each particle lies right on top of its initial position.

For the *case without initial neutron star spin* we use a 1.4 $\mathrm{M}_\odot$ neutron star that has been relaxed to equilibrium in isolation. This star is set (with the appropriate radial velocity) on an orbit with an angular frequency determined from the force balance condition (equation 14).

4 RESULTS

We performed six production runs with up to 10^6 SPH particles, exploring the dependence of the results on the mass ratio (q = 0.1, 0.3, 0.5) and on the initial neutron star spin (corotation and no initial spin). We follow the evolution for a long time (up to 64 ms corresponding to 300 dynamical time-scales of the initial neutron star; previous investigations (Lee & Kluzniak 1999a,b; Janka et al. 1999; Lee 2000, 2001) typically simulated ~20 ms). Details of the runs are shown in Table 1.

After an inspiral of typically one orbit, mass transfer sets in. In the corotating case, the mass from the neutron star is initially fed directly into the hole with mass transfer rates of several hundred $\mathrm{M}_\odot$ per second; see below. In agreement with the analytical estimates, the system without initial spin has less difficulties to bypass the Schwarzschild radius. Although somewhat easier in the irrotational case, we find it generally hard to form a massive accretion disc around the hole.

The dynamical evolution of run A (corotation, $q = 0.1$), run E (no spin, $q = 0.3$) and the extreme case run G (corotation, $q = 0.93$) are

Table 1. Summary of the different runs. C, corotation; I, no spin; a_0, initial separation; $T_{\rm sim}$, simulated duration; # part., total particle number.

Run	Mass ratio q	Spin	# part.	a_0 (km)	$T_{\rm sim}$ (ms)	Remark
A	0.1	C	292 427	105	63.8	
B	0.3	C	570 587	72	61.0	
C	0.5	C	292 427	60	55.6	
D	0.1	I	1 083 218	102	21.9	
E	0.3	I	1 083 218	69	26.5	
F	0.5	I	292 427	43.5	24.7	
G	0.93	C	102 831	48	39.5	extreme mass ratio
H	0.1	I	35513	100	20.2	polytrope, $\Gamma = 2$
I	0.1	I	35513	100	20.2	polytrope, $\Gamma = 3$

shown in Figs 4–6 [the logarithm of the column density (in g cm^{-2}) is colour-coded].

4.1 Black hole evolution

We plot in Fig. 7 the evolution of the mass transfer rates *into the hole* (in solar masses per second) and the evolution of the black hole masses for the corotating runs (runs A–C). For the smallest mass ratio, $q = 0.1$, there is one extreme initial mass transfer phase (see panel 2 in Fig. 4), in which around 1 M$_\odot$ is transferred within 5 ms into the hole, corresponding to a peak rate of more than 500 M$_\odot$ s^{-1}. After this phase the system undergoes six more mass transfer episodes in which the individual peak rates reach $\sim$0.8 M$_\odot$ s^{-1}; the hole mass increases only insignificantly during this phase. The larger mass ratio cases exhibit a shorter initial mass transfer, however, substantially more mass is accreted by the hole in the subsequent mass transfer episodes (see step-like behaviour in panel 2).

The mass transfer in the cases where the neutron star has no initial spin (see Fig. 8) is also dominated by the initial mass transfer episode with huge rates, again up to 500 M$_\odot$ s^{-1}. The rates in the subsequent phases, however, are typically two orders of magnitude lower so that the hole mass increases only marginally.

4.2 Disc

An accretion disc around a black hole is a vital ingredient for virtually all GRB models. Usually it is assumed that a neutron star–black hole merger is just a variant of neutron star binary mergers and produces even more massive (several 0.1 M$_\odot$), hot discs around the hole. We will show here that this assumption is – at least for our (hard) EOS and the simulate time-scale of several 10 ms – not justified.

Fig. 9 shows the SPH-particle densities in the inner region of run A (compare to the last panel in Fig. 4). The innermost part of the disc reaches densities of up to 10^{11} g cm^{-3} and contains a mass of only 7×10^{-3} M$_\odot$. The disc out to 600 km (red area in panel six of Fig. 4) contains 3×10^{-2} M$_\odot$. The interaction of the accretion stream with the disc is shown in Fig. 10. The mass-weighted temperatures of these disc regions are 2.5 and 1.4 MeV, respectively. This configuration is not very promising to launch a GRB, it can only anchor moderate magnetic fields and the neutrino emission is considerably lower than in the double neutron star case which can only produce GRBs of relatively low total energy output.

The other two corotating runs do not form any resolvable disc at all. The matter from the neutron star is transferred directly into the hole. From its backside mass is tidally removed. However, rather than forming a massive tidal tail like in the case of run A, this decompressed neutron star material forms a low-density common envelope around the orbiting neutron star–black hole system.

The case of $q = 0.3$ and no spin (run E) is shown in Fig. 5. Here the rest of the neutron star is orbiting inside a disc that is continually decreasing in density from values of 10^{10} g cm^{-3} between the hole and the neutron star to values of $\sim 10^5$ g cm^{-3} at a distance of 400 km from the hole. All the disc masses are very low, a few times 10^{-3} M$_\odot$, as still a lot of the total mass is retained in the orbiting mini neutron star. The (mass averaged) temperatures in these inner discs are only moderate, typically 3 MeV. Further details can be found in Table 2. Thus, none of the performed runs yields accretion disc that would be a convincing candidate to launch a GRB.

4.3 Neutron star evolution

The mass flow into the hole induces a sometimes violent fluid motion within the neutron star. To illustrate the difference for both spin cases, we plot the velocities in a frame that is momentarily rotating on a circular orbit (both the neutron star and black hole are lying on the x-axis) with the neutron star being at the origin. In this frame a perfectly corotating binary should only exhibit a radial velocity along the x-axis. We show in Fig. 11 two cases (corotating and no spin) where mass transfer has just set in. Note that the matter transferred towards the hole is coming from the neutron star backside. While the fluid figure of the corotating case is rather symmetric with respect to the x-axis, the irrotational case exhibits substantial perturbations on the front side of the neutron star.

The mass transfer induces high-amplitude (with respect to the neutron star radius) surface waves travelling with the sense of the orbital motion. They whip through the accretion stream connecting the neutron star with the hole, sometimes quenching the accretion stream. An example of such a phase is shown in Fig. 12 (same coordinate system as Fig. 11).

We find that in almost all cases the core of the neutron star survives all the mass transfer phases and continues to orbit the hole as a 'mini neutron star'. Only in our extreme (test) case with a black hole of 1.5 M$_\odot$ ($q = 0.93$) the neutron star is completely disrupted to form a hot and massive accretion disc.

4.4 Gravitational waves

If the more optimistic estimates for the neutron star–black hole merger rates are correct, these systems may be among the first sources to be detected by ground-based GW detectors. As will be shown below, the GW signal bears a clear imprint of the high-density nuclear matter EOS.

We show in Figs 13 and 14 the GW signatures of a run where a mini neutron star survives (run A) and of a case where the neutron star is finally completely disrupted. The first panel in each of the figures shows the mutual separation between the neutron star (defined as the centre of mass of the material with densities in excess of 10^{14} g cm^{-3}) and the black hole. After a smooth inspiral phase, the mass transfer (directly) into the hole sets in, which increases the orbital separation. The mini neutron star is then on a non-circular orbit and is further driven back to the hole by the GW back reaction. This sequence of mass transfer, moving out, coming back in, transferring mass to the hole again etc. continues until the end of the very long simulation. The existence of the mini neutron star is reflected in the GW luminosity: each periastron approach corresponds to a peak in the GW luminosity.

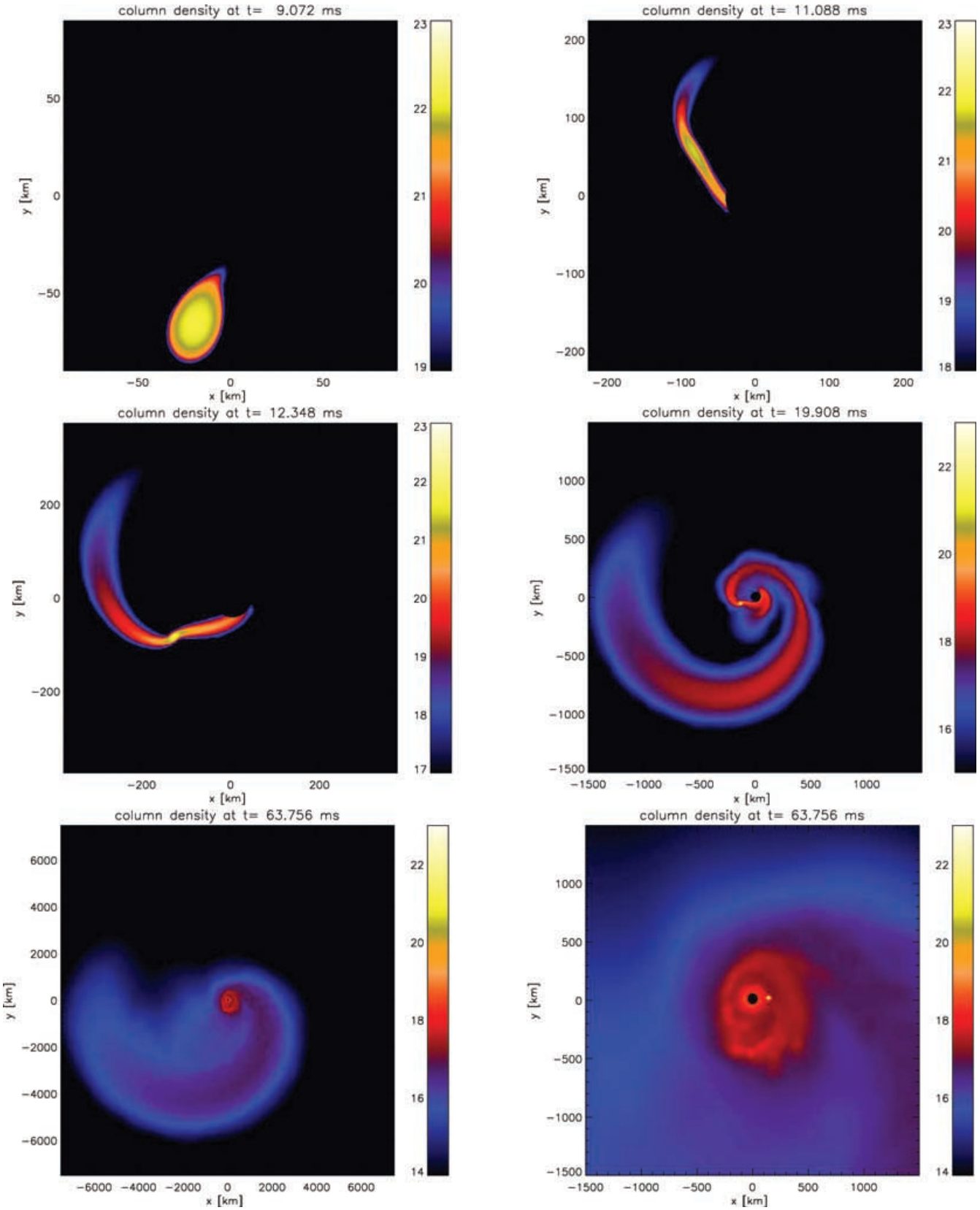

Figure 4. Dynamical evolution of run A (corotating neutron star, mass ratio $q = 0.1$). A 'mini neutron star' survives the encounter and keeps orbiting the central black hole. At the moment shown in panel 6 (= blow-up of panel 5) the mini neutron star has completed seven orbital revolutions. The column density is colour coded.

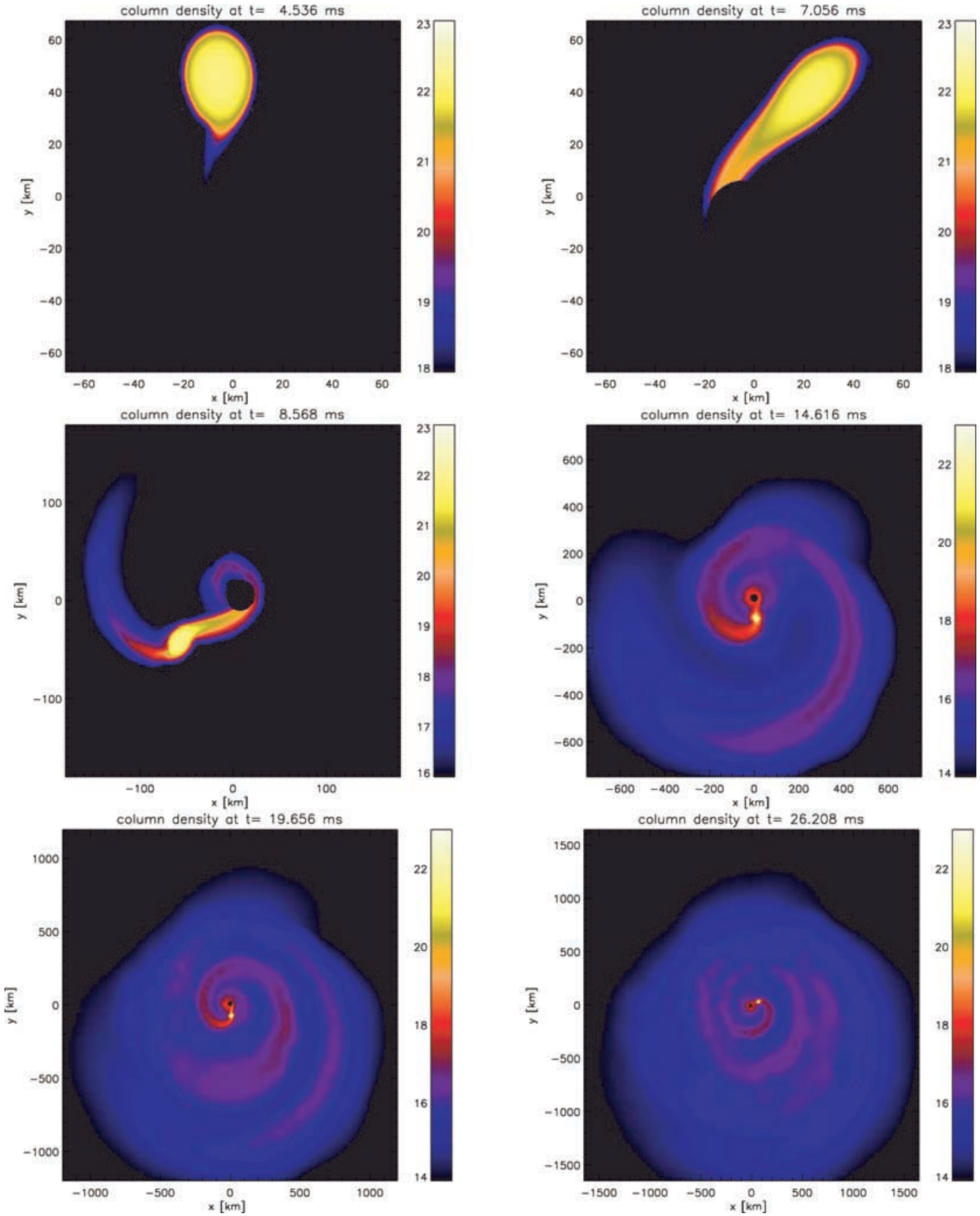

Figure 5. Evolution of run E (no neutron star spin, mass ratio $q = 0.3$).

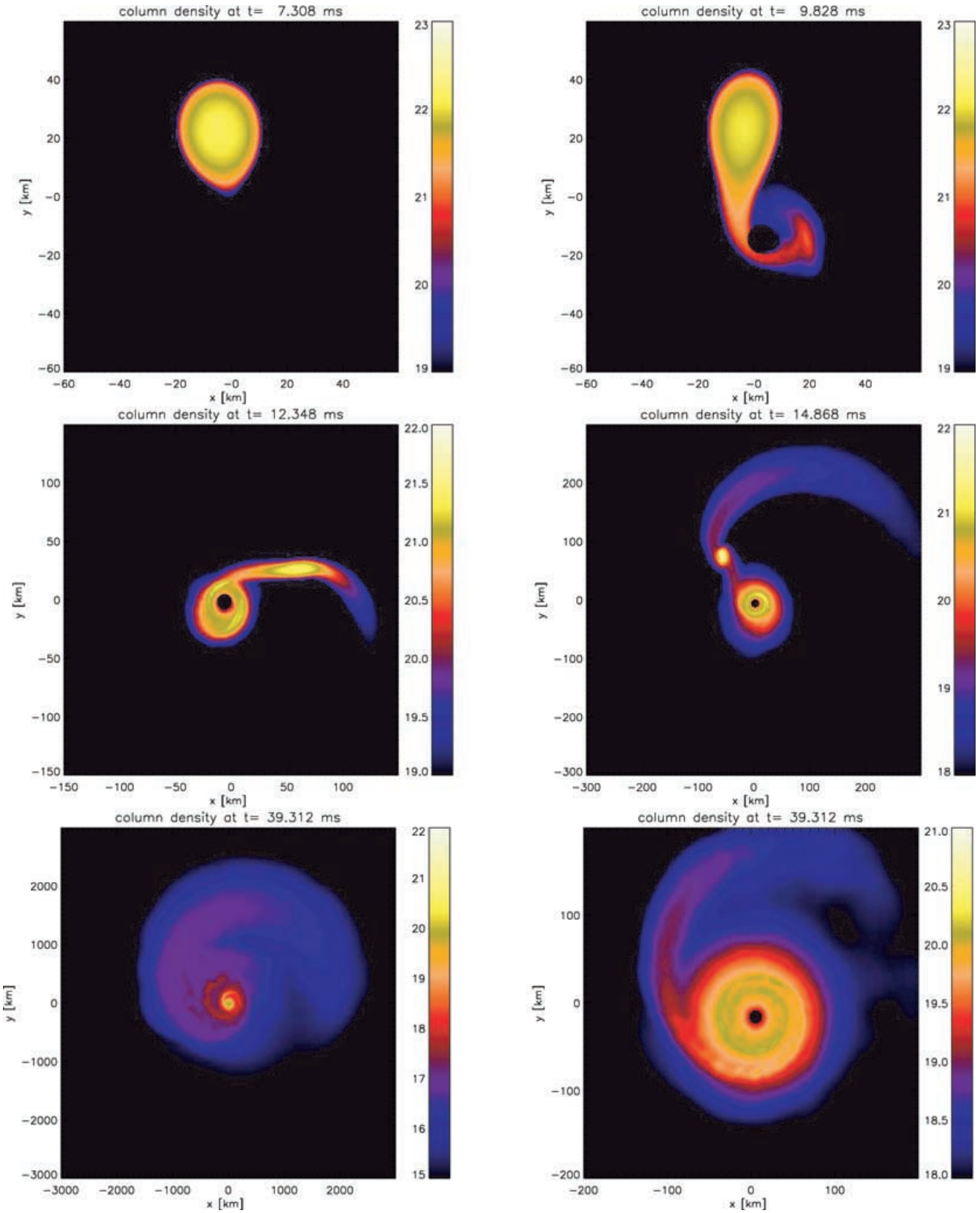

Figure 6. Evolution of the extreme case, run G (corotation, black hole with 1.5 $M_\odot$ and 1.4 $M_\odot$ neutron star). It is only in this case that the neutron star is completely disrupted and a very massive ($\sim$0.3 $M_\odot$) and hot (up to 10 MeV) accretion disc forms. Note that panel 6 shows a blow-up of the central region of panel 5.

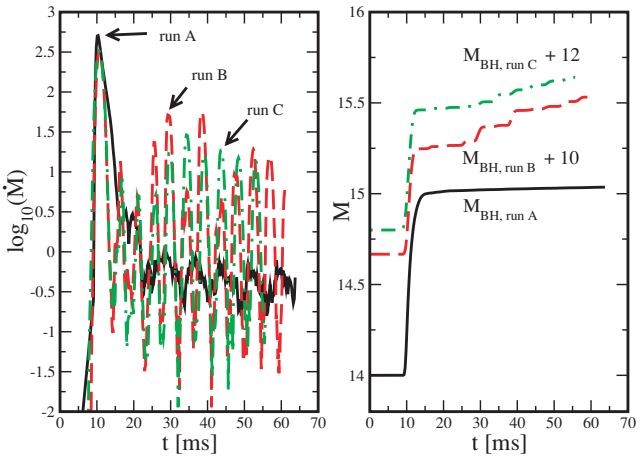

Figure 7. Evolution of the black hole for the corotating cases. The left panel shows the logarithm of the mass transfer rate *into the hole* (in solar masses per second), $\dot{M}$. The right panel shows the evolution of the black hole mass (in solar masses). Note that suitable offsets have been added to enhance the visibility of the mass increase.

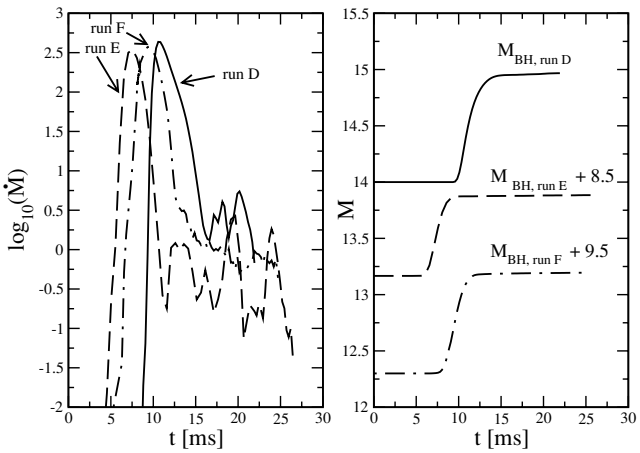

Figure 8. Same as in Fig. 7 but for the cases without neutron star spin (masses in solar units; offsets added to enhance visibility).

In our extreme case, run G, only three more close approaches (apart from the first one) are visible in the GW signal. The last encounter tidally disrupts the neutron star.

The survival of the neutron star is a direct consequence of the stiffness of the EOS. To prove this we have performed two low-resolution test runs with a soft ($\Gamma = 2$; run H) and a stiff ($\Gamma = 3$; run I) polytropic EOS. In the case of the soft EOS the neutron star is completely disrupted (see Fig. 15) while in the case with the stiff EOS, a mini neutron star survives (see Fig. 16). Thus, the GW signal serves as a direct probe of the poorly known regime of supranuclear densities.

5 SUMMARY AND DISCUSSION

We have performed simulations of the accretion dynamics in neutron star–black hole systems. Our simulations used a 3D smoothed particle hydrodynamics code together with the relativistic mean field nuclear EOS of Shen et al. (1998a,b) and a detailed neutrino scheme. Gravity was approximated with Newtonian forces plus back reaction from the emission of GWs.

Generally, we find a rather complex dynamics determined by the interplay between mass transfer (trying to increase the orbital separation), GW back reaction (acting to reduce the separation) and the reaction of the neutron star to mass loss. This reaction includes both the change of the neutron star radius and (in some cases) very violent fluid motions inside the star with amplitudes comparable to the stellar radius. In some of the cases the neutron star even seems to be close to fissioning into two fragments. Thus, a certain fraction of systems may result in a black hole orbited by two low-mass neutron stars. We find that many of the analytic estimates that are useful in other accreting systems are of limited use for neutron star–black hole systems. The overall evolution is very sensitive to the neutron star–black hole mass ratio.

We show generally that – if not superimposed by other effects such as a different tidal deformation or a different tidal lag angle – irrotational donor stars form easier accretion discs than corotating ones. This result is not restricted to neutron star–black hole systems, but holds generally. The reason is that in the irrotational case mass overflowing the L_1 Lagrange point has more specific angular momentum and therefore a larger circularization radius. In the neutron star–black hole case more material can avoid being fed directly into the Schwarzschild radius if the donor star is not spinning.

In the context of GRB progenitors neutron star–black hole systems are usually regarded only as a slight modification of the binary neutron star case. It is often stated that they will yield the 'standard GRB central engine', a black hole with a hot and massive accretion disc. Here, however, we find it very difficult to form such a disc. Although somewhat easier in the irrotational case, we find for all but extreme cases rather low-temperature discs ($\sim$3 MeV) of moderate densities, which are not promising to either launch a GRB via neutrino annihilation or via energy extraction from the black hole rotation with suitable magnetic field configurations. Some of our investigated systems do not form any resolvable discs at all. At the end of the simulation we have in these cases a binary system of a black hole and a low-mass neutron star engulfed in a common envelope of low-density material that has been tidally removed from the neutron star.

We find in all but extreme cases that the core of the initial star survives all mass transfer episodes as a 'mini neutron star'. Test runs with polytropic EOSs ($\Gamma = 2$ and $\Gamma = 3$) show that in the case of a stiff EOS a mini neutron star forms while a soft EOS leads to a complete tidal disruption of the neutron star. This result is consistent with the work of Lee (2000, 2001) and Lee & Kluzniak (1999a,b). Janka et al. (1999) also find in some cases that the core of the neutron star survives the initial mass transfer episodes but later on is completely disrupted. This is consistent with their EOS being somewhat softer than the one we use (for a comparison of both EOSs see fig. 5 of Rosswog & Davies 2002).

The survival of a mini neutron star and the difficulty to form a massive accretion disc are not unrelated; the surviving stellar core acts as some kind of storage that prevents mass from flowing towards the hole. Both effects are a result of the stiffness of the neutron star EOS as can be seen from an inspection of the test runs with a stiff (neutron star core, low-mass disc) and a soft polytropic EOS (complete disruption, more massive disc). Janka et al. (1999) found values for the neutrino emission and annihilation that are rather optimistic for GRBs. In both sets of simulations different numerical methods are used, but we regard the differences resulting from different techniques as minor. We consider the uncertainty in the basic physics at supranuclear densities and the sensitivity of the system dynamics to this part of the EOS to be the decisive factors for the differences in the results. There are not many equations of state

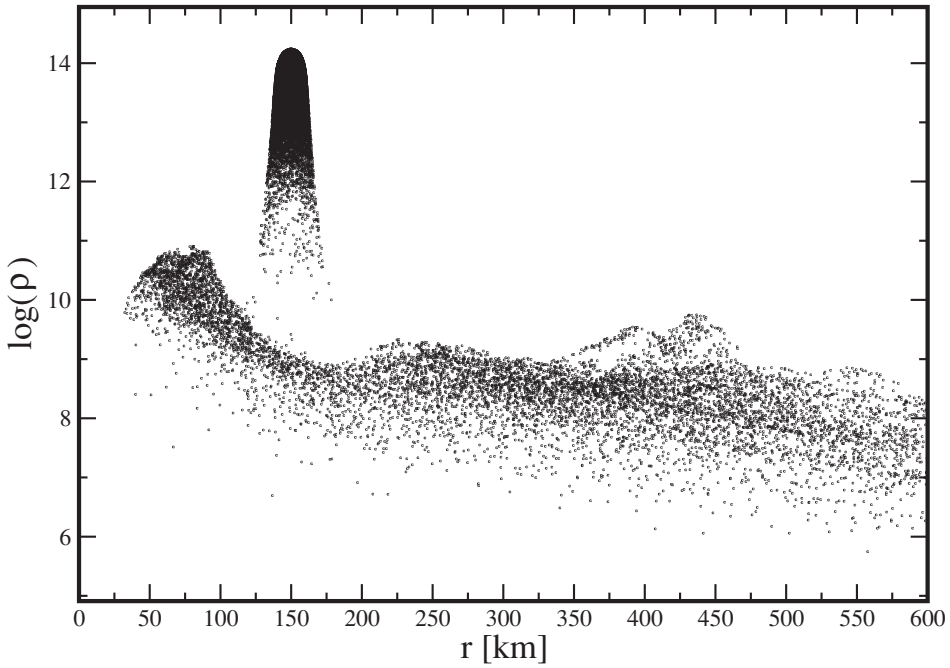

Figure 9. Logarithm of the densities of the SPH particles in the inner region of run A (corresponding to the last panel in Fig. 4). Clearly visible is the 'mini neutron star' at a radius of 150 km.

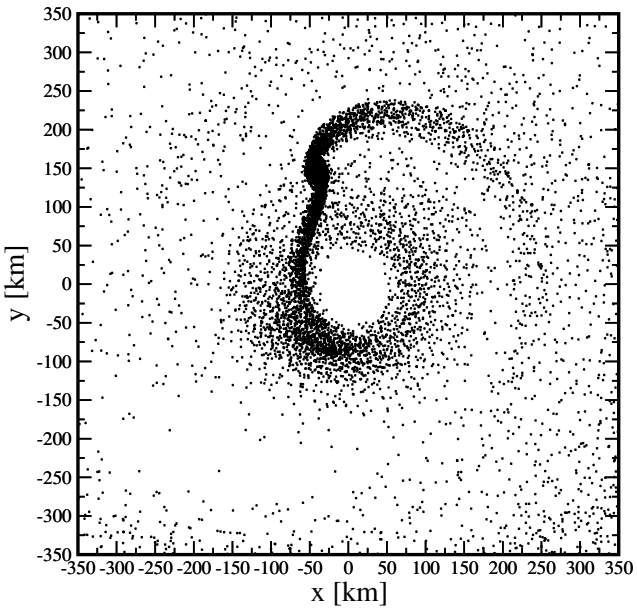

Figure 10. Interaction of the accretion stream with the disc (run A). Rather than a 'hot spot', such as in a cataclysmic variable, a 'hot band' across the disc is visible.

for the purpose of such simulations (temperature dependent, large range of densities, no β equilibrium assumed) available, the used examples of the Lattimer–Swesty EOS [simulations of Janka et al. (1999)] and the Shen EOS (our simulations) may therefore indicate the possible range of results as a function of the poorly known input physics.

In most cases huge tidal tails of decompressed neutron star material form. During the decompression phase the adiabatic exponent drops from values above 3 to values close to 4/3. This goes along with a recombination of nucleons into nuclei and therefore the release of several MeV per nucleon. These effects drive a rapid lateral expansion of the tidal tails that will therefore end up as large, structured discs around the hole.

Table 2. End of simulation: M_{14}, mass of orbiting mini neutron star; $M_{\rm disc}(T_{\rm sim})$, disc mass; $\langle T\rangle_{\rm disc}(T_{\rm sim})$, mass-averaged disc temperature; $L_{\rm GW}^{\rm max}$, peak GW luminosity; $\Delta E_{\rm GW}$, energy lost in GWs during the simulation time. In two of the cases no resolvable discs form.

Run	$M_{14}(T_{\rm sim})$ [$M_\odot$]	$M_{\rm disc}(T_{\rm sim})$ [$M_\odot$]	$\langle T\rangle_{\rm disc}(T_{\rm sim})$ [MeV]	$L_{\rm GW}^{\rm max}$ [erg s^{-1}]	$\Delta E_{\rm GW}$ [erg]
A	0.15	6.2×10^{-3} [a]	2.5	5.9×10^{55}	1.3×10^{53}
B	0.40	–	–	1.3×10^{55}	6.9×10^{52}
C	0.46	–	–	3.7×10^{54}	3.8×10^{52}
D	0.24	4.9×10^{-3}	2.7	4.7×10^{55}	1.7×10^{53}
E	0.68	2.3×10^{-3}	2.9	5.8×10^{54}	3.9×10^{52}
F	0.38	6.6×10^{-3}	3.9	6.5×10^{54}	3.1×10^{52}

Note: [a] 'inner disc', see text.

The GW luminosity reaches peak values close to 10^{56} erg s^{-1} at the first encounter. The survival of the mini neutron star leaves a clear imprint on the GW signature. All the subsequent periastron approaches yield a luminosity peak roughly two orders of magnitude below the value of the first close approach. In our extreme case with mass ratio close to 1, both the amplitude and luminosity die off abruptly once the mini neutron star is finally disrupted. Thus a softening of the EOS at supranuclear densities owing to, for example, hyperon condensates would be directly observable in the GW signature of a neutron star–black hole system.

ACKNOWLEDGMENTS

It is a pleasure to thank the Leicester supercomputer team Stuart Poulton, Chris Rudge and Richard West for their excellent support.

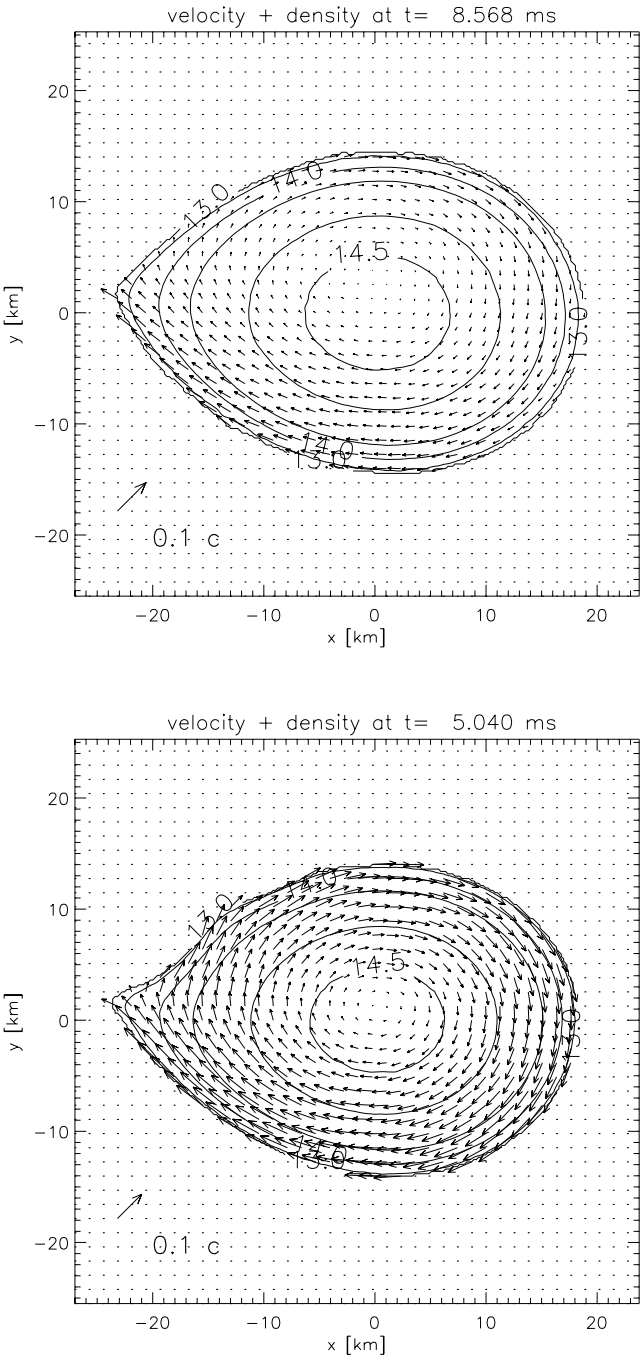

Figure 11. Comparison of the velocity fields at the beginning mass transfer. The velocities are plotted in a frame that is on a circular orbit with a velocity equal to the tangential velocity of the star (x-axis through black hole and neutron star, neutron star at origin). The upper panel refers to a corotating star (run B, $q = 0.3$), the lower one to the case without initial spin (run E, $q = 0.3$).

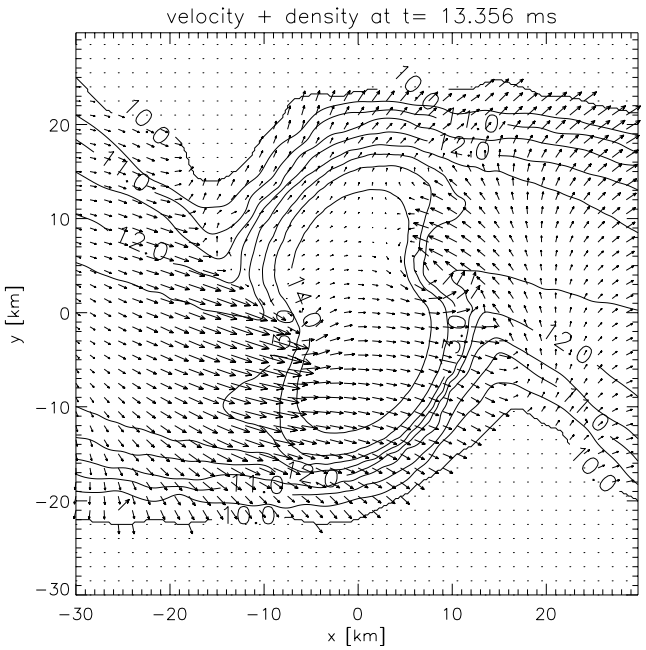

Figure 12. Fluid motions inside the neutron star induced by the mass transfer (same coordinate system as in Fig. 11). Snapshot from run D (no spin, $q = 0.1$), the contour lines refer to $\log(\rho)$.

Most of the computations reported here were performed using the UK Astrophysical Fluids Facility (UKAFF). Part of this work has been performed using the supercomputer of the University of Leicester Mathematical Modelling Centre which was purchased through the EPSRC strategic equipment initiative.

This work was supported by a PPARC Rolling Grant for Theoretical Astrophysics. SR gratefully acknowledges the support via a PPARC Advanced Fellowship. RS whishes to thank the UK Astrophysical Fluid Facility (UKAFF) in Leicester for the kind hospitality during a visit, where parts of this work were accomplished, and he would like to acknowledge the funding of this visit by the EU FP5 programme.

REFERENCES

Balsara D., 1995, J. Comput. Phys., 121, 357
Belczynski K., Kalogera V., Bulik T., 2002, ApJ, 572, 407
Benz W., 1990, in Buchler J., ed., Numerical Modeling of Stellar Pulsations. Kluwer Academic Publishers, Dordrecht, p. 269
Bildsten L., Cutler C., 1992, ApJ, 400, 175
Centrella J. M., McMillan S. L. W., 1993, ApJ, 416, 719
Eggleton P. P., 1983, ApJ, 268, 368
Eichler D., Livio M., Piran T., Schramm D. N., 1989, Nat, 340, 126
Freiburghaus C., Rosswog S., Thielemann F. K., 1999, ApJ, 525, L121
Janka H. T., Eberl T., Ruffert M., Fryer C. L., 1999, ApJ, 527, 39
Kippenhahn R., Weigert A., 1990, Stellar Structure and Evolution. Springer, Berlin
Lattimer J., Schramm D. N., 1974, ApJ, 192, L145
Lattimer J., Schramm D. N., 1976, ApJ, 210, 549
Lattimer J., Swesty D., 1991, Nucl. Phys. A, 535, 331
Lattimer J., Mackie F., Ravenhall D. G., Schramm D. N., 1977, ApJ, 213, 225
Lee W. H., 2000, MNRAS, 318, L606
Lee W. H., 2001, MNRAS, 328, 583
Lee W. H., Kluzniak W. L., 1999a, ApJ, 526, 178
Lee W. H., Kluzniak W. L., 1999b, MNRAS, 308, 780
Mészáros P., 2002, ARA&A, 40, 137
Misner C., Thorne K., Wheeler J. A., 1973, Gravitation. W. H. Freeman & Co., New York
Monaghan J., Gingold R., 1983, J. Comp. Phys., 52, 374
Monaghan J. J., 1992, ARA&A, 30, 543
Narayan R., Pazcynski B., Piran T., 1992, ApJ, 395, L83
Paczynski B., 1992, Acta Astron., 41, 257
Plavec M., Kratochvil P., 1964, Bull. Astron. Inst. Czech., 15, 165

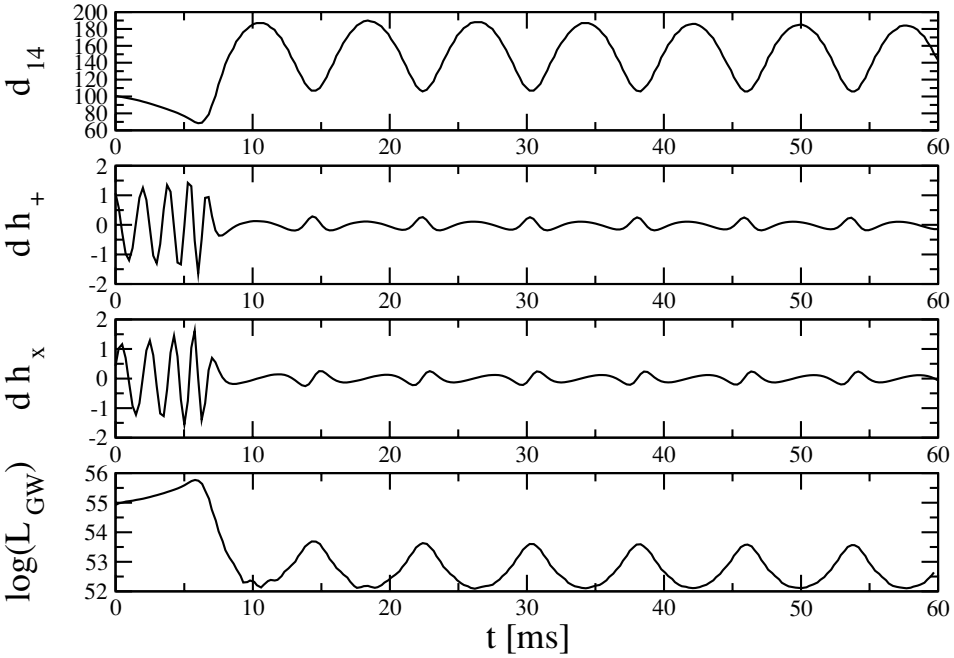

Figure 13. GW emission of run A ($q = 0.1$, corotating neutron star). The upper panel shows the separation of the neutron star (defined via a density threshold of 10^{14} g cm^{-3}) and the black hole. Panels 2 and 3 show the gravitational amplitudes h_+ and h_x (d is the distance to the observer) and the last panel gives the GW luminosity. In this run the mini neutron star survives the whole simulated time, the periastron approaches are clearly visible in the GW luminosity.

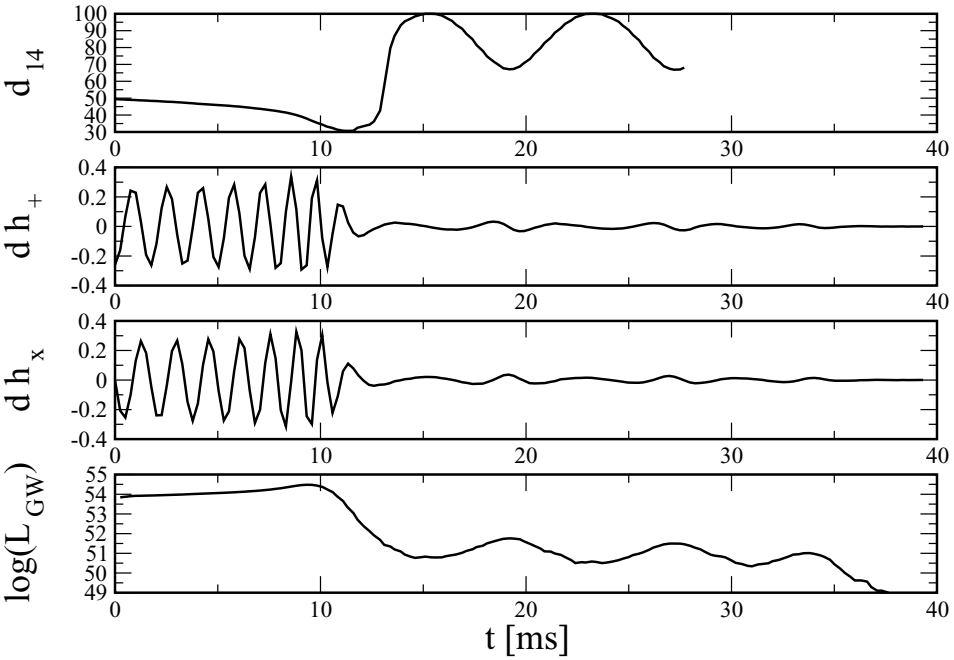

Figure 14. Same as Fig. 13 for run G. This is the only case where the neutron star is completely disrupted. At 27 ms the peak density drops below the threshold of 10^{14} g cm^{-3} (end of curve in panel 1), at 35 ms the neutron star has completely disappeared and the GW luminosity drops to essentially zero.

Piran T., 1999, Phys. Rep., 314, 575
Rosswog S., Davies M.-B., 2002, MNRAS, 334, 481
Rosswog S., Liebendörfer M., 2003, MNRAS, 342, 673
Rosswog S., Liebendörfer M., Thielemann F.-K., Davies M. B., Benz W., Piran T., 1999, A&A, 341, 499
Rosswog S., Davies M. B., Thielemann F.-K., Piran T., 2000, A&A, 360, 171
Ruffert M., Janka H. T., Schäfer G., 1996, A&A, 311, 532
Shen H., Toki H., Oyamatsu K., Sumiyoshi K., 1998a, Nucl. Phys., A, 637, 435
Shen H., Toki H., Oyamatsu K., Sumiyoshi K., 1998b, Prog. Theor. Phys., 100, 1013
Symbalisty E. M. D., Schramm D. N., 1982, Astrophys. Lett., 22, 143
Zhuge X., Centrella J., McMillan S., 1996, Phys. Rev. D, 54, 7261

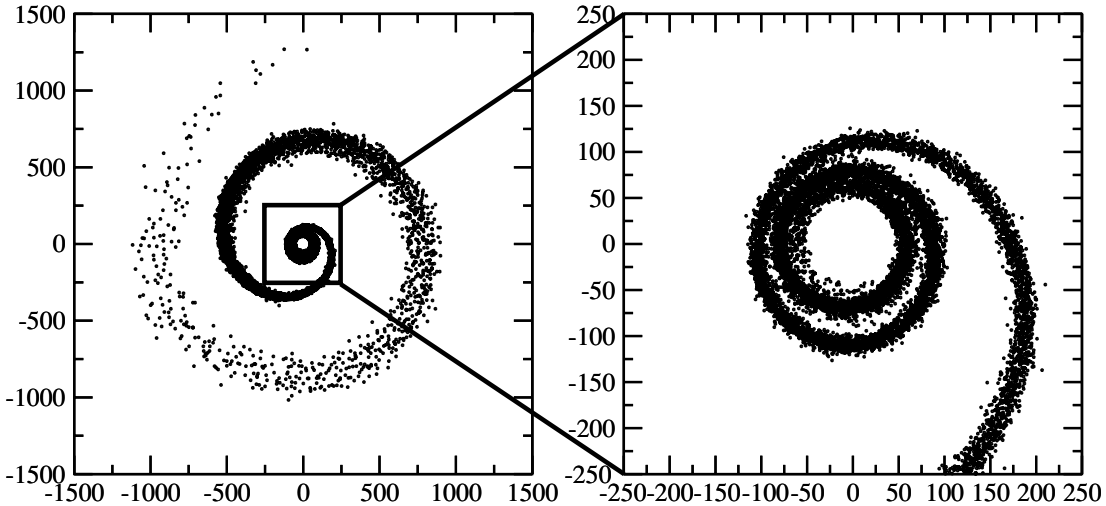

Figure 15. SPH-particle position (at $t = 18.4$ ms) of the low-resolution test run with a soft ($\Gamma = 2$) polytropic EOS: the neutron star is completely disrupted.

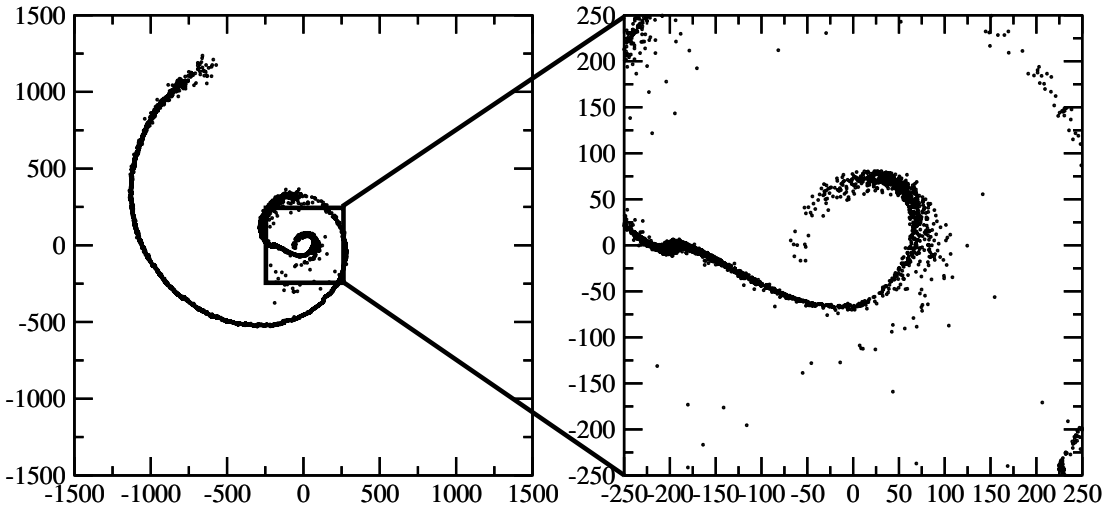

Figure 16. SPH-particle position (at $t = 18.4$ ms) of the low-resolution test run with a stiff ($\Gamma = 3$) polytropic EOS: a mini neutron star survives.

APPENDIX A: GRAVITATIONAL WAVES

We treat GWs in the quadrupole approximation (see e.g. Misner, Thorne & Wheeler 1973). The reduced quadrupole moments can be written in terms of SPH-particle properties (Centrella & McMillan 1993)

$$I_{jk} = \sum_i m_i \left[x_{ji} x_{ki} - \frac{1}{3}\delta_{jk}(r^i)^2 \right]. \tag{A1}$$

The second time-derivatives, $\ddot{I}_{jk}$, can be expressed in terms of particle properties by straight forward differentiation. For the third-order time-derivatives we use the analytical derivatives of a cubic spline interpolation of the $\ddot{I}_{jk}$. The retarded GW amplitudes for a distant observer along the binary axis at distance d are given by

$$dh_+ = \frac{G}{c^4}(\ddot{I}_{xx} - \ddot{I}_{yy}) \tag{A2}$$

and

$$dh_\times = 2\frac{G}{c^4}\ddot{I}_{xy}, \tag{A3}$$

the total GW luminosity is approximated as

$$L_{\rm GW} \cong \frac{G}{5c^5} I^{(3)}_{jk} I^{(3)}_{jk}, \tag{A4}$$

where the superscript denotes the third derivative with respect to time.

This paper has been typeset from a TEX/LATEX file prepared by the author.